

Manipulation of the Landé g-factor in InAs quantum dots through the application of anisotropic gate potentials: Exact diagonalization, numerical and perturbation methods

Sanjay Prabhakar,¹ James E. Raynolds² and Roderick Melnik^{1,3}

¹*M²NeT Laboratory, Wilfrid Laurier University, Waterloo, ON, N2L 3C5 Canada*

²*Sterne, Kessler, Goldstein & Fox P.L.L.C., 1100 New York Avenue, NW, Washington, DC 20005*

³*Department of Mathematical Information Technology, University of Jyväskylä, 40014, Finland*

(Dated: September 27, 2011)

We study the variation in the Landé g-factor of electron spins induced by both anisotropic gate potentials and magnetic fields in InAs quantum dots for possible implementation towards solid state quantum computing. In this paper, we present analytical expressions and numerical simulations of the variation in the Landé g-factor for both isotropic and anisotropic quantum dots. Using both analytical techniques and numerical simulations, we show that the Rashba spin-orbit coupling has a major contribution in the variation of the g-factor with electric fields before the regime, where level crossing or anticrossing occurs. In particular, the electric field tunability is shown to cover a wide range of g-factor through strong Rashba spin-orbit interaction. Another major result of this paper is that the anisotropic gate potential gives quenching effect in the orbital angular momentum that reduces the variation in the E-field and B-field tunability of the g-factor if the area of the symmetric and asymmetric quantum dots is held constant. We identify level crossings and anticrossings of the electron states in the variation of the Landé g-factor. We model the wavefunctions of electron spins and estimate the size of the anticrossing for the spin states $|0, -1, +1/2\rangle$ and $|0, 0, -1/2\rangle$ corresponding to a quantum dot that has been recently studied experimentally (Phys. Rev. Lett. **104**, 246801 (2010)).

I. INTRODUCTION

Single electron spins in an electrostatically defined quantum dot in a 2-dimensional electron gas (2DEG) have been manipulated and studied by several groups.¹⁻⁷ Quantum dots in III-V type semiconductors provide an opportunity to study the variation in the Landé g-factor vs. gate potentials and magnetic fields.⁸⁻¹³ The shape and size of the quantum dots can be modified by changing the gate controlled electric fields that influence the variation in the energy spectrum as well as the Landé g-factor of the dots.^{3,14,15} The results of this research might enhance the opportunities of building spintronic logic devices for possible implementation towards solid state quantum computing.¹⁶⁻²⁰

The orbital and spin angular momentum of the electron in a semiconductor quantum dot interact through the Rashba and Dresselhaus spin-orbit couplings.^{21,22} These two spin-orbit coupling effects arise from two different types of symmetry operations in III-V type semiconductors. The Rashba spin-orbit coupling arises from the structural inversion asymmetry of the triangular shaped quantum well confining potential. The Dresselhaus spin-orbit coupling arises from bulk inversion asymmetry. The mathematical expressions for the Rashba and Dresselhaus spin-orbit couplings that are implemented into the theoretical model are given in this paper in Section II. The strength of the Rashba and Dresselhaus spin-orbit couplings is determined by the gate controlled electric fields and is an important parameter in controlling the Landé g-factor for both isotropic and anisotropic quantum dots.

The goal of the present work is to explore the non-

degenerate energy spectrum of electrostatically defined InAs quantum dot by both analytical techniques and numerical simulations. These approaches provide realistic information for controlling the Landé g-factor for both isotropic and anisotropic quantum dots through the application of gate potentials. We also model realistic wavefunctions of electrons in InAs quantum dots that were recently studied by experimentalists in Ref. 23. We estimate the size of avoided anticrossing is approximately 65 μeV , which is in agreement with the experimentally reported values.²³ In this paper, by utilizing both analytical and numerical techniques, we find that the Rashba spin-orbit coupling produces the dominant effect on the variation of the Landé g-factor vs. electric field strength below the level crossing or anticrossing. Also, anisotropic gate potential lead to a quenching effect in the orbital angular momentum that reduces the variation in the g-factor. Our work is similar to those of Refs. 3, 4, 5, 24, 25 and 26 but differs in that we utilize both analytical and numerical approaches based on the finite element method.

The paper is organized as follows. In Sec. II, we exactly diagonalize the Hamiltonian of a quantum dot confined in an asymmetric potential including spin-orbit interaction and a magnetic field along z-direction. In Sec. III, based on a second order perturbation calculation, we present analytical expressions of the Landé g-factor for both isotropic and anisotropic quantum dots. In Sec. IV, we plot the Landé g-factor induced by gate controlled electric fields vs. magnetic field as well as quantum dot radii for pure Rashba case ($\alpha_D = 0$), pure Dresselhaus case ($\alpha_R = 0$) and mixed cases (both α_R, α_D present) where α_R and α_D are two parameters related to the

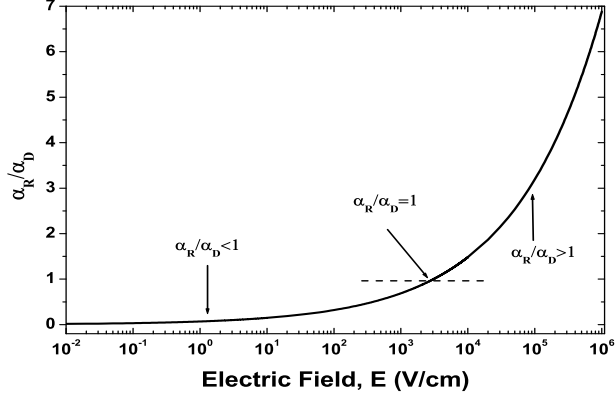


FIG. 1. Contributions of Rashba and Dresselhaus spin-orbit couplings (α_R/α_D) vs. Electric Field. It can be seen that Rashba and Dresselhaus spin-orbit couplings becomes equal at the electric field, $E = 3.05 \times 10^3$ V/cm. This plot is obtained from Eq. 9.

strength of the Rashba and Dresselhaus spin-orbit interactions respectively. We also model the wavefunctions of electron states that were recently reported by experimentalists in Ref. 23. Finally, in Sec. V, we summarize our results.

II. THEORETICAL MODEL

The Hamiltonian of an electron in a quantum dot in the plane of a 2DEG, in the presence of an external magnetic field along z-direction can be written as^{7,27}

$$H = H_{xy} + H_{so}, \quad (1)$$

where the Hamiltonian H_{so} is associated to the Rashba-Dresselhaus spin-orbit couplings and H_{xy} is the Hamiltonian of the electron along the lateral direction in the plane of the 2DEG. H_{xy} can be written as

$$H_{xy} = \frac{\vec{P}^2}{2m} + \frac{1}{2}m\omega_o^2(ax^2 + by^2) + \frac{1}{2}g_o\mu_B\sigma_z B, \quad (2)$$

where $\vec{P} = \vec{p} + e\vec{A}$ is the kinetic momentum operator, $\vec{p} = -i\hbar(\partial_x, \partial_y, 0)$ is canonical momentum operator and $\vec{A} = \frac{B}{a+b}(-yb, xa, 0)$ is the vector potential in the asymmetric gauge. Here, $-e < 0$ is the electronic charge, m is the effective mass of the electron in the conduction band, μ_B is the Bohr magneton, σ_z is the Pauli spin matrix along z-direction. Also, $\omega_o = \frac{\hbar}{m\ell_o^2}$ is a parameter characterizing the strength of the confining potential and ℓ_o is used as the radius of the quantum dot. By choosing the appropriate values of a and b , one can define the shape of the quantum dot from circle to ellipse. The Hamiltonian H_{xy} can be exactly diagonalized (see Appendix A) by writing the Hamiltonian as a function of number operators $n_{\pm} = a_{\pm}^{\dagger}a_{\pm}$ and its energy spectrum can be written as,²⁸

$$\varepsilon_{n_+n_-} = (n_+ + n_- + 1)\hbar\omega_+ + (n_+ - n_-)\hbar\omega_- + \frac{1}{2}g_o\mu_B\sigma_z B, \quad (3)$$

$$a_{\pm} = \frac{1}{(s_+ - s_-)(1+i)} \left[\pm(s_{\mp} \pm i)\frac{\ell}{\hbar}p_x + (s_{\pm} \pm i)\frac{\ell}{\hbar}p_y + (1 \mp is_{\mp})\frac{1}{\ell}x \pm (1 \mp is_{\pm})\frac{1}{\ell}y \right], \quad (4)$$

$$a_{\pm}^{\dagger} = \frac{1}{(s_+ - s_-)(1-i)} \left[\pm(s_{\mp} \mp i)\frac{\ell}{\hbar}p_x + (s_{\pm} \mp i)\frac{\ell}{\hbar}p_y + (1 \pm is_{\mp})\frac{1}{\ell}x \pm (1 \pm is_{\pm})\frac{1}{\ell}y \right], \quad (5)$$

where,

$$s_{\pm} = \frac{\omega_{\pm}}{\omega_c\sqrt{\frac{\Omega_2}{\Omega_1}}} \left[\frac{\Omega_2}{\Omega_1} - 1 \pm \sqrt{\frac{\omega_c^2\Omega_2}{\omega_{\pm}^2\Omega_1} + \left(1 - \frac{\Omega_2}{\Omega_1}\right)^2} \right], \quad (6)$$

$$\omega_{\pm} = \frac{1}{2} \left[\omega_c^2 + (\Omega_1 \pm \Omega_2)^2 \right]^{1/2}, \quad (7)$$

provided that $[a_{\pm}, a_{\pm}^{\dagger}] = 1$ and $[x, p_x] = [y, p_y] = i\hbar$. Here $\Omega_1 = \omega_0\sqrt{a}$, $\Omega_2 = \omega_0\sqrt{b}$, $\ell = \sqrt{\frac{\hbar}{m\Omega}}$, $\Omega = \sqrt{\omega_0^2 + \frac{1}{4}\omega_c^2}$ and $\omega_c = \frac{eB}{m}$ is the cyclotron frequency. Note that a similar type of expression for the energy spectrum of an anisotropic quantum dot is also discussed

in Ref. 26. However, our methodology for diagonalizing the Hamiltonian is slightly different (see in Appendix A). Also, we verified that by substituting $a = b = 1$, Eqs. (3-6) are exactly the same as those in Ref. 7. The eigenstates of H_{xy} in Eq. 2 with $a = b = 1$ are well-known Fock-Darwin energy states.^{29,30}

The Hamiltonian associated with the spin-orbit couplings can be written as^{21,22}

$$H_{so} = \frac{\alpha_R}{\hbar}(\sigma_x P_y - \sigma_y P_x) + \frac{\alpha_D}{\hbar}(-\sigma_x P_x + \sigma_y P_y). \quad (8)$$

The spin-orbit Hamiltonian consists of the Rashba coupling whose strength is characterized by the parameter α_R and the Dresselhaus coupling with α_D . These coupling parameters depend on the electric field E of the

quantum well confining potential (i.e., $E = -\partial V/\partial z$) along z direction at the interface in a heterojunction as

$$\alpha_R = \gamma_R e E, \quad \alpha_D = 0.78 \gamma_D \left(\frac{2me}{\hbar^2} \right)^{2/3} E^{2/3}, \quad (9)$$

$$H_{so} = \alpha_R (1+i) \left[b^{1/4} \kappa_+ (s_+ - i) a_+ + b^{1/4} \kappa_+ (s_- + i) a_- + a^{1/4} \eta_- (i - s_-) a_+ + a^{1/4} \eta_- (i + s_+) a_- \right] \\ + \alpha_D (1+i) \left[a^{1/4} \kappa_- (i - s_-) a_+ + a^{1/4} \kappa_- (i + s_+) a_- + b^{1/4} \eta_+ (-i + s_+) a_+ + b^{1/4} \eta_+ (i + s_-) a_- \right] + h.c., \quad (10)$$

where,

$$\kappa_{\pm} = \frac{1}{2(s_+ - s_-)} \left\{ \frac{1}{\ell} \sigma_x \pm i \frac{eB\ell}{\hbar} \left(\frac{1}{\sqrt{a} + \sqrt{b}} \right) \sigma_y \right\}, \\ \eta_{\pm} = \frac{1}{2(s_+ - s_-)} \left\{ \frac{1}{\ell} \sigma_y \pm i \frac{eB\ell}{\hbar} \left(\frac{1}{\sqrt{a} + \sqrt{b}} \right) \sigma_x \right\},$$

and h.c. represents the hermitian conjugate. It is clear that the spin-orbit Hamiltonian and the Zeeman spin splitting energy in both isotropic and anisotropic quantum dots obeys a selection rule in which the orbital angular momentum can change by one quantum.

III. ANALYTICAL EXPRESSION FOR THE LANDÉ g-FACTOR

Our conventional definition of the electron g-factor in the conduction band in the presence of magnetic field along z-direction can be written as^{5,7}

$$g = \frac{\varepsilon_{0,0,+1/2} - \varepsilon_{0,0,-1/2}}{\mu_B B}, \quad (11)$$

where $\varepsilon_{0,0,+1/2}$ and $\varepsilon_{0,0,-1/2}$ are the eigenvalues of the electron in the conduction band with spin up and down respectively having the lowest orbital angular momentum.

At low electric fields and small quantum dot radii, we treat the Hamiltonian associated to the Rashba and Dresselhaus spin-orbit couplings as a perturbation. Based on second order perturbation theory, the energy of the elec-

tron spin states can be written as, where the Rashba coefficient $\gamma_R = 110 \text{ \AA}^2$, Dresselhaus coefficient $\gamma_D = 130 \text{ eV \AA}^3$ and effective mass $m = 0.0239$ have been considered for InAs quantum dots.⁷

The Rashba and Dresselhaus spin-orbit Hamiltonian can be written in terms of raising and lowering operators as:⁷

$$\varepsilon_{0,0,+1/2} = \varepsilon_{0,0,+1/2}^{(0)} + \varepsilon_{0,0,+1/2}^{(2)}, \quad (12)$$

$$\varepsilon_{0,0,-1/2} = \varepsilon_{0,0,-1/2}^{(0)} + \varepsilon_{0,0,-1/2}^{(2)}. \quad (13)$$

The zero order energy correction can be easily calculated from Eq. (3). The first order energy correction is zero. The calculation for the second order energy correction can be written as:

$$\varepsilon_{0,0,+1/2}^{(2)} = \frac{\alpha_R^2 \xi_+ + \alpha_D^2 \varsigma_+}{\varepsilon_{0,0,+1/2}^{(0)} - \varepsilon_{1,0,-1/2}^{(0)}} + \frac{\alpha_R^2 \xi_- + \alpha_D^2 \xi_-}{\varepsilon_{0,0,+1/2}^{(0)} - \varepsilon_{0,1,-1/2}^{(0)}}, \quad (14)$$

$$\varepsilon_{0,0,-1/2}^{(2)} = \frac{\alpha_R^2 \varsigma_+ + \alpha_D^2 \xi_+}{\varepsilon_{0,0,-1/2}^{(0)} - \varepsilon_{1,0,1/2}^{(0)}} + \frac{\alpha_R^2 \xi_- + \alpha_D^2 \varsigma_-}{\varepsilon_{0,0,-1/2}^{(0)} - \varepsilon_{0,1,+1/2}^{(0)}}, \quad (15)$$

where,

$$\xi_{\pm} = \frac{1}{2(s_+ - s_-)} \left\{ \pm \frac{1}{s_{\pm}} \alpha_{\pm}^2 + 2\alpha_{\pm} \beta_{\pm} \mp \frac{1}{s_{\mp}} \beta_{\pm}^2 \right\}, \quad (16)$$

$$\varsigma_{\pm} = \frac{1}{2(s_+ - s_-)} \left\{ \pm \frac{1}{s_{\mp}} \alpha_{\mp}^2 - 2\alpha_{\mp} \beta_{\mp} \mp \frac{1}{s_{\mp}} \beta_{\mp}^2 \right\}, \quad (17)$$

$$\alpha_{\pm} = a^{1/4} \left\{ \frac{1}{\ell} \pm \frac{eB\ell}{\hbar} \frac{1}{(\sqrt{a} + \sqrt{b})} \right\}, \quad (18)$$

$$\beta_{\pm} = b^{1/4} \left\{ \frac{1}{\ell} \pm \frac{eB\ell}{\hbar} \frac{1}{(\sqrt{a} + \sqrt{b})} \right\}. \quad (19)$$

By substituting Eqs. 12 and 13 in Eq. 11, the expression for the Landé g-factor of anisotropic quantum dots can be written as,

$$g_{\text{asym}} = g_0 - \frac{1}{\mu_B B} \left\{ \frac{\alpha_R^2 \xi_+ + \alpha_D^2 \varsigma_+}{\hbar \omega_x - \Delta} + \frac{\alpha_R^2 \xi_- + \alpha_D^2 \xi_-}{\hbar \omega_y - \Delta} - \frac{\alpha_R^2 \varsigma_+ + \alpha_D^2 \xi_+}{\hbar \omega_x + \Delta} - \frac{\alpha_R^2 \xi_- + \alpha_D^2 \varsigma_-}{\hbar \omega_y + \Delta} \right\}. \quad (20)$$

In the above expression, we use the relation $\omega_x = \omega_+ +$

ω_- , $\omega_y = \omega_+ - \omega_-$ and $\Delta = g_0 \mu_B B$. By substituting

$a = b = 1$ in Eq. 20, one find the Landé g-factor for isotropic quantum dot:

$$g_{sym} = g_0 + 2 \frac{m_e m}{\hbar^4} [\alpha_D^2 (1 - \delta) - \alpha_R^2 (1 + \delta)] \ell_0^2 - \frac{1}{2} \frac{m_e m^3}{\hbar^6} \left[\alpha_D^2 \left(\frac{1}{2} - \frac{1}{2} \delta + \delta^2 + \delta^3 \right) - \alpha_R^2 \left(\frac{1}{2} + \frac{1}{2} \delta + \delta^2 - \delta^3 \right) \right] \omega_c^2 \ell_0^6 + \dots, \quad (21)$$

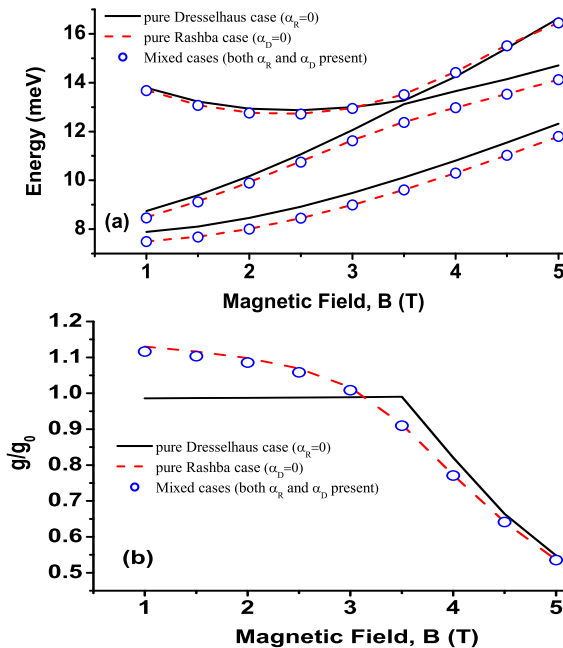


FIG. 2. (Color online) (a) Eigenenergy levels for ground, first and second excited states vs. magnetic fields. (b) Effective Landé g-factor vs. magnetic fields. In both cases, solid lines represent pure Dresselhaus case ($\alpha_R = 0$), dashed lines represent pure Rashba case ($\alpha_D = 0$) and open circles represent mixed cases (both α_R and α_D present). Also in both cases, we choose the electric field $E = 3 \times 10^3$ V/cm and the quantum dot radius, $\ell_0 = 20$ nm for symmetric quantum dots ($a = b = 1$).

where $g_0 = -15$ is the bulk g-factor for InAs quantum dots and $\delta = g_0 m / m_e$. Here m_e is the mass of electron. The analytical expressions for the Landé g-factor of both anisotropic and isotropic quantum dots in Eqs. (20) and (21) respectively are valid before the level crossing or anticrossing occurs. It can be seen that the g-factor for both isotropic and anisotropic quantum dots depends on the anisotropic gate potentials, quantum dot radii and magnetic fields. These are our control parameters in manipulating the g-factor for both isotropic and anisotropic quantum dots.

IV. RESULTS AND DISCUSSIONS

We have used the Finite Element Method³¹ to solve numerically the corresponding eigenvalue problem with Hamiltonian given by Eq. (1) to study the variation in the Landé g-factor at high electric fields for the values $\alpha_R/\alpha_D > 1$, large quantum dot radii and magnetic fields for both isotropic ($a = b$) and anisotropic ($a \neq b$) quantum dots. Throughout the simulations, unless otherwise stated, we consider $\ell_0 = 20$ nm for g/g_0 vs. magnetic field and $B = 1$ T for g/g_0 vs. quantum dot radius. Our numerical simulations related to the g-factor in quantum dots are valid before the level crossing or anticrossing occurs. At or after the level crossing or anticrossing, g-factor simply captures the effects of two lowest eigenstates in quantum dots.

In Fig. 1, we investigate the strength of the Rashba and Dresselhaus spin-orbit interactions vs. electric fields. The strength of the Rashba and Dresselhaus spin-orbit couplings for InAs quantum dots can be determined by the relation $\alpha_R/\alpha_D = 0.015E^{1/3}$ (see Eq. 9). From this relation, it can be found that both Rashba and Dresselhaus spin-orbit couplings become equal at the electric field $E = 3.05 \times 10^3$ V/cm. However, at this value of the electric field where $\alpha_R = \alpha_D$, the rotational symmetry is not broken and the spin splitting energy mainly corresponds to the Zeeman energy. For $E = 10^4$ V/cm to 10^6 V/cm, α_R/α_D varies from 1.5 to 6.88 (see Fig. 1). Since $\alpha_R/\alpha_D > 1$, only the Rashba spin-orbit coupling has an appreciable contribution to spin splitting energy.

Figure 2 illustrates the eigenenergy of the states $|0, 0, +1/2\rangle$, $|0, 0, -1/2\rangle$, and $|0, -1, +1/2\rangle$ and g-factor vs. magnetic fields of symmetric quantum dots ($a = b = 1$) for pure Rashba ($\alpha_D = 0$, solid lines), pure Dresselhaus ($\alpha_R = 0$, dashed lines) and mixed cases (both α_R and α_D present, open circles). It can be seen that the Dresselhaus spin-orbit coupling has almost no effect on the manipulation of the g-factor. For the pure Dresselhaus case, we find a level crossing at 3.5 T. However, for the pure Rashba and mixed spin-orbit couplings, we find an avoided anticrossings in the manipulation of the g-factor.

Figure 3 explores the variation of several eigenenergy states and the g-factor vs. magnetic field for a symmetric quantum dot ($a = b = 1$). In Fig. 3(a), we plot several eigenenergy levels (ground, first, etc.) vs. magnetic field for symmetric quantum dots with gate induced electric

fields $E = 10^4$ V/cm (solid lines) and $E = 5 \times 10^5$ V/cm (dashed lines). Here we find level crossing shown by open circles at magnetic field, $B = 3.5$ T for the electric field $E = 10^4$ V/cm (solid lines). However, we find an anticrossing for electric field $E = 5 \times 10^5$ V/cm (dashed lines). The symbol \times in Fig. 3 (a) represents the data from perturbation theory which is in agreement with the numerical simulations. In Fig. 3(b), we plot the Landé g-factor vs. magnetic field at the electric fields $E = 10^4$ V/cm (solid lines), 3×10^5 V/cm (dashed lines), 5×10^5 V/cm (dotted lines), 7×10^5 V/cm (dashed-dotted lines) and 10^6 V/cm (dashed-dotted-dotted lines) for a symmetric quantum dot. It is clear that there is a level crossing between the states $|0, 0, -1/2\rangle$ and $|0, -1, +1/2\rangle$ in the manipulation of the g-factor at $B = 3.5$ T for $E = 10^4$ V/cm (solid lines). However, with the increase in the electric field, we have an anticrossing in the variation of the g-factor. This is also consistent with previously published work by R. de Sousa and S. Das Sarma⁷ and we consider this result as a benchmark for our computational work.

In Fig. 4, we analyze anisotropy effects on the variation of the eigenenergy and of the Landé g-factor vs. magnetic fields. In Fig. 4(a), we plot the eigenenergy vs. magnetic field for quantum dots in the potentials characterized by $a = b = 1$ (solid lines), $a = b = 3$ (dashed lines) and $a = 1, b = 9$ (dotted lines). Here, we choose $E = 10^4$ V/cm. We find a level crossing at $B = 3.5$ T for the symmetric quantum dot ($a = b = 1$). However, the level crossing extends approximately to $B = 6.2$ T for the symmetric quantum dots ($a = b = 3$). The extension of the level crossing to the larger magnetic fields is mainly due to the increase on the lateral size of the quantum dots. We quantify that the area of the quantum dots with ($a = b = 3$) is 9 times larger than the dots with ($a = b = 1$). For anisotropic quantum dots with the potential ($a = 1, b = 9$), we find the level crossing at around $B = 6$ T. Note that the area of the asymmetric dots in the potential ($a = 1, b = 9$) is exactly equal to the area of the symmetric dots with the potential ($a = b = 3$). In Fig. 4(b) and (c), we plot the variation in the Landé g-factor vs. magnetic field for quantum dots in the confining potentials of $a = b = 3$ and $a = 1, b = 9$. In both cases, we choose the electric fields as same as in Fig. 3(b). In Fig. 4 (b) for symmetric quantum dots ($a=b=3$), we find a crossover point (all the curves collapse to a single point) at around $B = 5$ T. However, this point decreases to approximately $B = 4.5$ T for asymmetric quantum dots ($a=1, b=9$) as shown in Fig. 4(c). At this point, the value of g-factor is equal to the bulk g-value of InAs dots (i.e., $g = g_0 = -15$) for all gate induced electric fields. Also, in Fig. 4(c), we see that the anisotropic potential gives a quenching effect in the orbital angular momentum that reduces the electric field tunability of the g-factor.

Finally, Fig. 5 illustrates the manipulation of the Landé g-factor vs. quantum dot radii for both symmetric and asymmetric quantum dots. Again, the electric fields are chosen as same as in Fig. 3(b). In Fig. 5(a) and

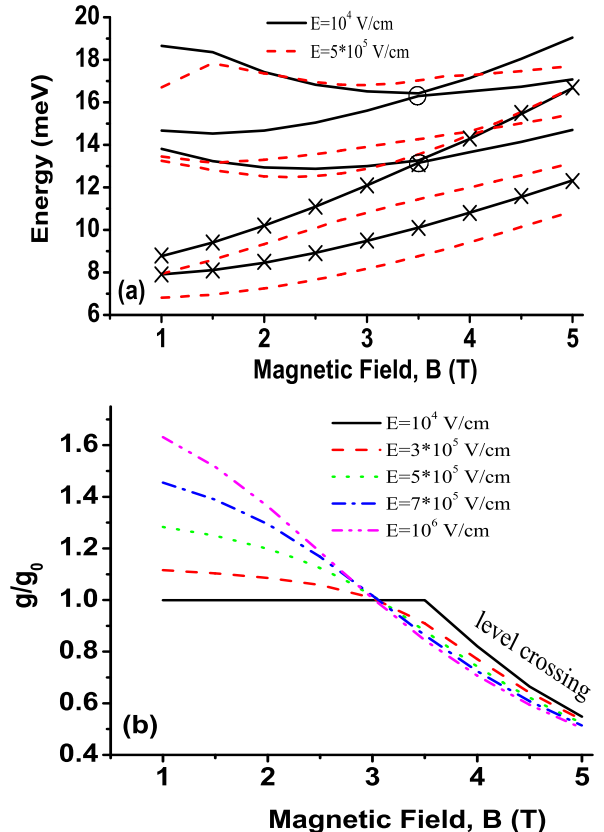


FIG. 3. (Color online) (a) Several eigenenergy levels vs. magnetic fields at the electric fields: $E = 10^4$ V/cm (solid lines) and $E = 5 \times 10^5$ V/cm (dashed lines). The symbol \times represents data from perturbation theory. A level crossing occurs at the magnetic field, $B = 3.5$ Tesla for the electric field, $E = 10^4$ V/cm (solid line) and is shown by open circles. (b) Effective Landé g-factor vs. magnetic field at the electric fields $E = 10^4$ V/cm (solid line), 3×10^5 V/cm (dashed line), 5×10^5 V/cm (dotted line), 7×10^5 V/cm (dashed-dotted line) and 10^6 V/cm (dashed-dotted-dotted line). In (a) and (b), we choose the quantum dot radius, $\ell_0 = 20$ nm for symmetric quantum dots ($a = b = 1$).

(b), we consider isotropic confining potentials: $a = b = 1$ and $a = b = 3$. In Fig. 5(b), level crossing point extends to the larger quantum dot radii compared to that of Fig. 5(a) mainly due to the increase in the lateral size of the quantum dots. In Fig. 5(c), we capture the anisotropic effect of the E-field tunability of the g-factor vs. quantum dot radii with the potential $a = 1, b = 9$. Again, we see that the anisotropic potential $a = 1, b = 9$ (Fig. 5(c)) reduces the E-field tunability compared to that of isotropic potential $a = b = 3$.

Now we consider the wavefunctions and estimate the size of the anticrossing point in an experimentally re-

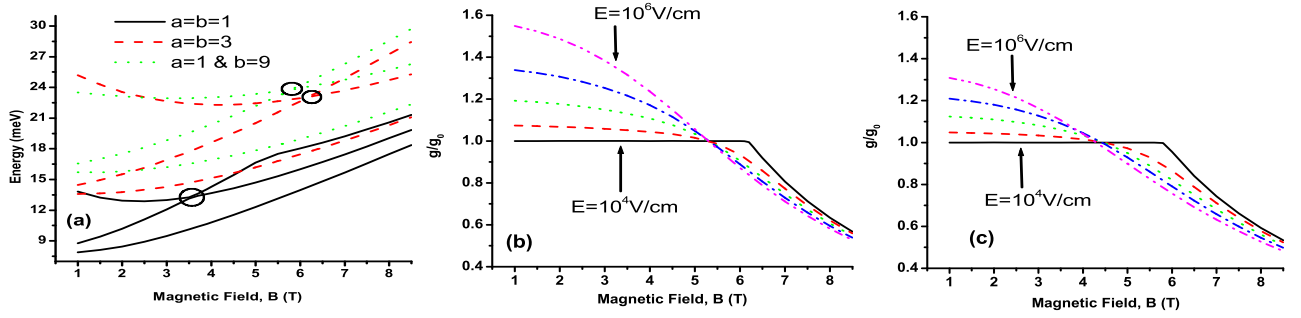


FIG. 4. (Color online) (a) Several eigenenergy levels vs. magnetic field at the electric field $E = 10^4$ V/cm for both symmetric ($a = b = 1$ (solid lines), $a = b = 3$ (dashed lines)) and asymmetric quantum dots ($a = 1, b = 9$, (dotted lines)). In (b) and (c), we plot effective Landé g-factor vs. magnetic fields. The electric fields are chosen as same as in Fig. 3(b). Also, in (b) and (c), we choose $a = b = 3$ and $a = 1, b = 9$ respectively. In all cases, we choose the quantum dot radius, $\ell_0 = 20$ nm.

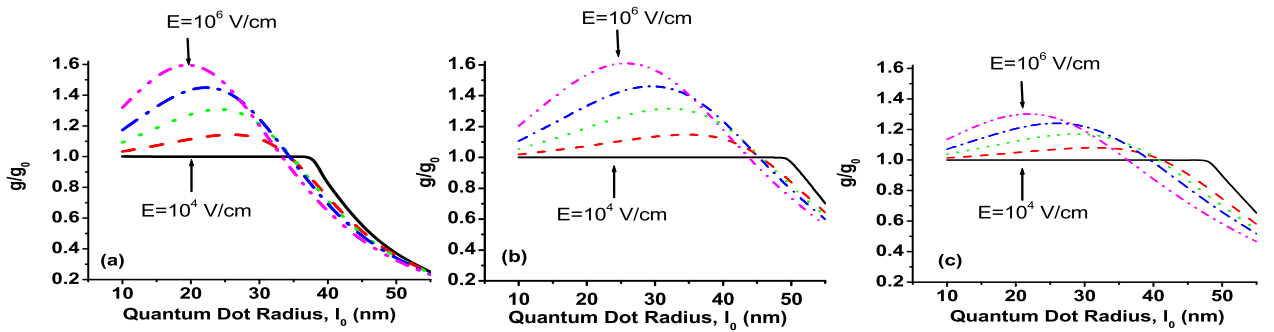


FIG. 5. (color online) Landé g-factor vs. quantum dot radius for both symmetric ($a = b$) and asymmetric ($a \neq b$) quantum dots. Again, the electric fields are chosen as same as in Fig. 3(b). Also we choose $a = b = 1$, $a = b = 3$ and $a = 1, b = 9$ in (a),(b) and (c) respectively. In all cases, we consider the magnetic field $B = 1$ T.

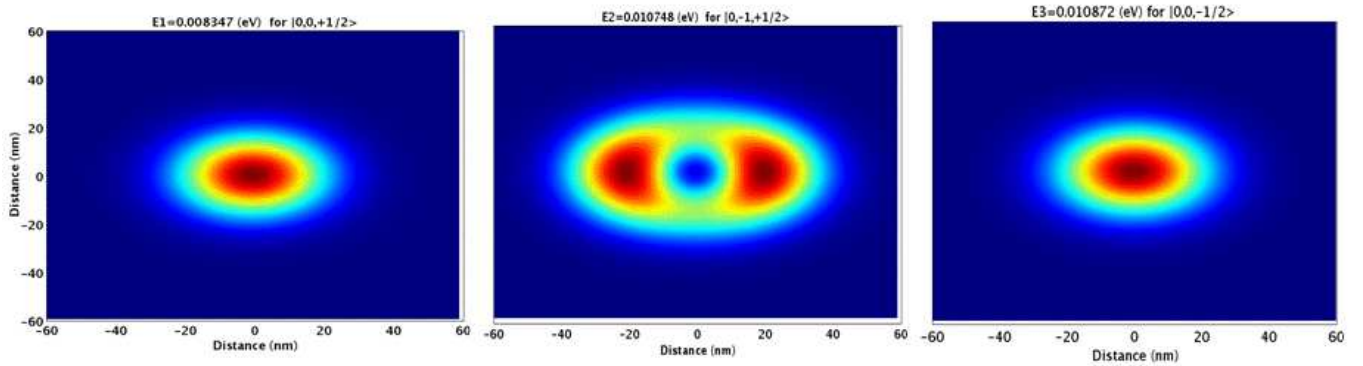


FIG. 6. (color online) In-plane wavefunctions in an asymmetric quantum dot. Here we choose $a = 1.5$, $b = 4$, $E = 1.6 \times 10^4$ V/cm, $B = 2.9$ T and $\ell_0 = 28$ nm. These parameters mimic the wavefunctions of the quantum states $|0, 0, +1/2\rangle$, $|0, -1, +1/2\rangle$ and $|0, 0, -1/2\rangle$ (from left to right) in Ref. 23 of Fig.(2a).

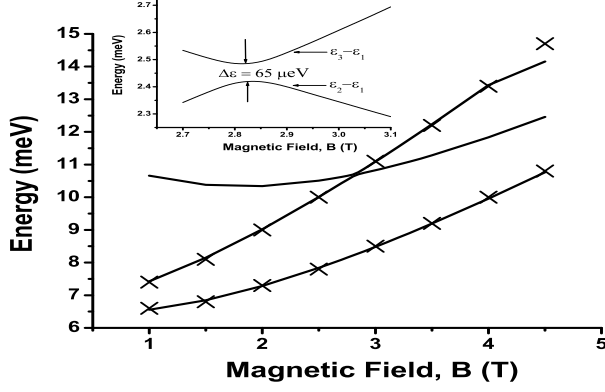


FIG. 7. Eigenenergy of electron states $|0, 0, +1/2 \rangle$, $|0, -1, +1/2 \rangle$ and $|0, 0, -1/2 \rangle$ vs. magnetic field. The symbol \times represents the data from perturbation theory. The inset shows the energy difference vs. magnetic field near the level crossing point. Here we estimate the size of the anti-crossing point to be approximately $65 \mu eV$. Here we again consider $a = 1.5$, $b = 4$, $E = 1.6 \times 10^4$ V/cm, and $\ell_0 = 28$ nm.

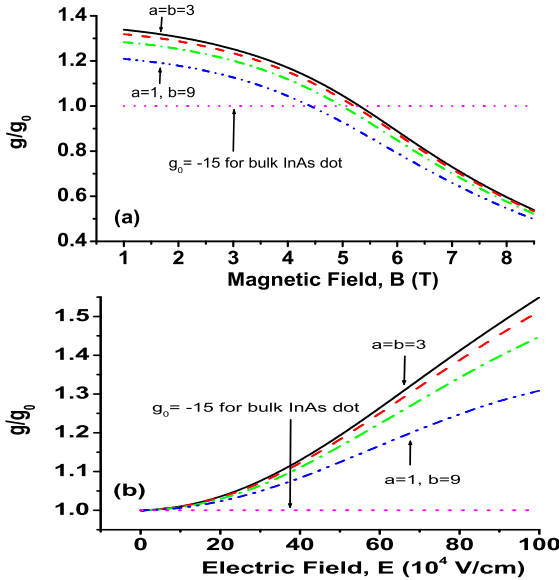


FIG. 8. (Color online) Manipulation of the Landé g -factor vs. magnetic and electric fields for quantum dots in the potential characterized by (top to bottom) $a = b = 3$ (solid lines), $a = 2$, $b = 4.5$ (dashed lines), $a = 1.5$, $b = 6$ (dashed-dotted line) and $a = 1$, $b = 9$ (dashed-dotted-dotted lines). We consider electric field, $E = 7 \times 10^5$ V/cm in case (a) and magnetic fields $B = 1$ T in case (b). In both cases, we consider the quantum dot radius $\ell_0 = 20$ nm.

ported self assembled InAs quantum dot in Ref. 23. The authors in Ref. 23 characterize the lateral size of the quantum dots by two anisotropic gate potentials, $\hbar\omega_x = 1.5$ meV and $\hbar\omega_y = 4$ meV. This anisotropic potentials give 46 nm lateral size of the quantum dots along the x-axis and 28 nm along the y-axis in the plane of 2DEG. By substituting $a = 1.5$, $b = 4$ and $\ell_0 = 28$ nm in our theoretical model, this will mimic the experimentally reported values of the lateral size of the quantum dots. The authors in Ref. 23 also report that the height of the pyramidal shape quantum dots is 20 nm. In our theoretical model, the quantum dot is formed in the plane of 2DEG so we choose the average height of the quantum dots as 10 nm. In very crude approximation, this thickness of the 2DEG is their height of the pyramidal shape quantum dots.³² Now, the expression $(2meE/\hbar^2)^{-1/3}$ in our theoretical model gives an estimate of the thickness of 2DEG which basically defines the size of the quantum dot along z-direction. 10 nm vertical size of the quantum dot in the above expression gives an estimate of the electric fields, $E = 1.6 \times 10^4$ V/cm. We find the anti-crossing point at around $B = 2.9$ Tesla and consider this value to capture the realistic wavefunctions for the states $|0, 0, +1/2 \rangle$, $|0, 0, -1/2 \rangle$ and $|0, -1, 1/2 \rangle$. From Fig. 6, the first excited state wavefunction is $|0, -1, +1/2 \rangle$ which is a clear indication of the level crossing point. In Fig. 7, we plot eigenenergy of the electron states $|0, 0, +1/2 \rangle$, $|0, -1, +1/2 \rangle$ and $|0, 0, -1/2 \rangle$ vs. magnetic field. Again, the symbol \times in Fig. 7 represents the data from perturbation theory for asymmetric potentials which is in agreement with the numerical simulations. It can be seen that there is an anticrossing point at the magnetic field of around 2.9 Tesla. Theoretically investigated level crossing point ($B=2.9$ T) is slightly smaller than the experimentally reported values ($B=3.5$ T, see Ref. 23) which indicates that the characterization of the lateral size of the quantum dots by anisotropic potentials has an estimate error of 20%. The inset plot shows the magnified image near the level crossing point. Here we estimate the size of the anticrossing to be nearly $65 \mu eV$ which is in agreement with the experimentally reported values in Ref. 23.

In Fig. 8, we summarize our results for the manipulation of the Landé g -factor with respect to both magnetic and electric fields in isotropic and anisotropic quantum dots. In Fig. 8(a), we plot the g -factor vs. magnetic field at $E = 7 \times 10^5$ V/cm. Also, we plot the g -factor vs. electric field at $B = 1$ T in Fig. 8(b). In both cases, we compare the result for isotropic quantum dots ($a = b = 3$, solid lines) and for anisotropic quantum dots $a = 2, b = 4.5$ (dashed lines), $a = 1.5, b = 6$ (dashed-dotted lines) and $a = 1, b = 9$ (dashed-dotted-dotted lines). Note that the quantum dots in the above confining potentials have the same area. At large magnetic fields, $B \sim 5$ T in Fig. 8(a) and small electric fields, $E \sim 10^5$ V/cm in Fig. 8(b), the effect of the resulting spin and orbital angular momentum of the quantum states on the eigenvalues ($\varepsilon_{0,0,+1/2} - \varepsilon_{0,0,-1/2}$) are small, leading

towards the bulk g-factor *i.e.* $g/g_0 \sim 1$ or $g = -15$. However, at small magnetic fields, $B \sim 1$ T in Fig. 8(a) and large electric fields, $E \sim 10^6$ V/cm in Fig. 8(b), the effect on $(\varepsilon_{0,0,+1/2} - \varepsilon_{0,0,-1/2})$ is large enough to drag the g-factor towards the free electron value *i.e.* $g/g_0 \sim 2$. Also, in both cases, if we compare the g-factor in both isotropic and anisotropic quantum dots, we find that anisotropic potentials ($a \neq b$) give the quenching effect in the orbital angular momentum that reduces the variation in the B-field tunability and E-field tunability of the Landé g-factor. This is also expected from Eqs. 20 and 21. For example, suppose $B = 1$ T, $\ell_0 = 20$ nm and $E = 3 \times 10^5$ V/cm. Then from Eq. 20, we find $g_{asym} = 1.04$ for anisotropic quantum dots ($a = 1, b = 9$). However, from Eq. 21, we find $g_{sym} = 1.07$ for isotropic quantum dots ($a = b = 3$). Also in Fig. 8 (a) and (b), it can be seen that $g_{sym} > g_{asym}$. Again, this quantitative analysis is in excellent agreement with our numerical simulations.

V. CONCLUSIONS

By utilizing both analytical expressions and numerical simulations (based on Finite Element Method), from Figs. 1-5, we have shown that the Rashba spin-orbit coupling has the major contribution on the variation of the g-factor with electric fields before the level crossing or anticrossing occurs. In Fig. 6, we have demonstrated the results of modeling of the realistic wavefunctions of the states $|0, 0, +1/2\rangle$, $|0, -1, +1/2\rangle$ and $|0, 0, -1/2\rangle$ near the level crossing point and estimate $65 \mu\text{eV}$ as the size of the anticrossing in Fig. 7. Finally, in Fig. 8, we have shown that the anisotropic gate potential gives the quenching effect in the orbital angular momentum that reduces the variation in the B-field tunability and E-field tunability of the g-factor.

ACKNOWLEDGMENTS

This work was supported by NSERC and CRC program, Canada.

Appendix A: Energy spectrum of asymmetric quantum dot

The Hamiltonian of an electron in a quantum dot in the plane of a 2DEG can be written as

$$H_{xy} = \frac{\vec{P}_x^2 + \vec{P}_y^2}{2m} + \frac{1}{2}m\omega_o^2(ax^2 + by^2). \quad (\text{A1})$$

The Eq. (A1) can be exactly diagonalized²⁸ by making a canonical transformation of position and momentum operators as

$$x_1 = \sqrt{\frac{\Omega_1}{\omega_0}} x, \quad P_1 = \sqrt{\frac{\omega_0}{\Omega_1}} P_x, \quad (\text{A2})$$

$$x_2 = \sqrt{\frac{\Omega_2}{\omega_0}} y, \quad P_2 = \sqrt{\frac{\omega_0}{\Omega_2}} P_y, \quad (\text{A3})$$

where $\Omega_1 = \omega_0\sqrt{a}$ and $\Omega_2 = \omega_0\sqrt{b}$. Also, the Gauge potential can be written as

$$A_x = -\frac{x_2 B \sqrt{\Omega_2 \omega_0}}{\Omega_1 + \Omega_2}, \quad A_y = \frac{x_1 B \sqrt{\Omega_1 \omega_0}}{\Omega_1 + \Omega_2}. \quad (\text{A4})$$

Substituting Eqs. (A2, A3, A4) into Eq. (A1), we get the Hamiltonian in the form of:

$$H_{xy} = \frac{\Omega_1}{2m\omega_0} [P_1^2 + x_1^2 + e(P_2^2 + x_2^2) + c(x_1 P_2 - x_2 P_1)]. \quad (\text{A5})$$

The abbreviations used in Eq. (A5) are as follows:

$$e = \Omega_2/\Omega_1, \quad c = \left(2\omega_c\sqrt{\Omega_2/\Omega_1}\right) / \left[\omega_c^2 + (\Omega_1 + \Omega_2)^2\right]^{1/2}.$$

Also we use the relation $m\omega_0\gamma = 1$, where $\gamma^2 = 1 + \left[\omega_c^2 / (\Omega_1 + \Omega_2)^2\right]$.

The energy spectrum of Hamiltonian (A5) can be found as follows. First, we need to find the canonical transformation U of the four-dimensional phase space, $P^t \equiv (P_x, P_y, x, y)$ which diagonalizes the quadratic form of the Hamiltonian (A5). To be more specific, Hamiltonian (A1) can be written as

$$H_{xy} = \left(\frac{\Omega_1}{2m\omega_0}\right) P^t M P, \quad \mathbf{M} = \begin{pmatrix} 1 & 0 & 0 & -c/2 \\ 0 & e & c/2 & 0 \\ 0 & c/2 & 1 & 0 \\ -c/2 & 0 & 0 & e \end{pmatrix}, \quad (\text{A6})$$

where t represents the transpose of a vector. The orthogonal unitary matrix U which exactly diagonalizes the matrix M can be written as,

$$\mathbf{U} = \frac{1}{(s_+ - s_-)} \begin{pmatrix} 1 & 1 & -s_- & -s_+ \\ 1 & -1 & s_+ & -s_- \\ s_- & s_+ & 1 & 1 \\ -s_+ & s_- & 1 & -1 \end{pmatrix}, \quad (\text{A7})$$

where $cs_{\pm} \equiv e - 1 \pm d$ and

$$d = \sqrt{\frac{4\omega_c^2\Omega_2/\Omega_1}{\omega_c^2 + (\Omega_1 + \Omega_2)^2} + \left(1 - \frac{\Omega_2}{\Omega_1}\right)^2}. \quad (\text{A8})$$

Also, the expression for s_{\pm} is written in Eq. (6). In terms of rotated operators $P' = UP$, the Hamiltonian (A6) can be written as

$$H_{xy} = \left(\frac{\Omega_1}{2m\omega_0}\right) \left[\frac{1}{2}(cs_- + 2)(p_x'^2 + x'^2) + \frac{1}{2}(cs_+ + 2)(p_y'^2 + y'^2) \right].$$

The above Hamiltonian is identified as the superposition of two independent harmonic oscillators and its energy spectrum can be written as

$$\varepsilon_{n_+n_-} = (n_+ + n_- + 1)\hbar\omega_+ + (n_+ - n_-)\hbar\omega_-, \quad (\text{A9})$$

provided that $\left[a_{\pm}^{\dagger}, a_{\pm} \right] = 1$. Also $\omega_{\pm} = \frac{1}{2} \left[\omega_c^2 + (\Omega_1 \pm \Omega_2)^2 \right]^{1/2}$.

- ¹ S. Bandyopadhyay, Phys. Rev. B **61**, 13813 (2000).
- ² D. D. Awschalom, D. Loss and N. Samarth, Semiconductor Spintronics and Quantum Computation, Springer, Berlin (2002).
- ³ S. Prabhakar and J. E. Reynolds, Phys. Rev. B **79**, 195307 (2009).
- ⁴ S. Prabhakar, J. E. Reynolds, A. Inomata and R. Melnik, Phys. Rev. B **82**, 195306 (2010).
- ⁵ C. E. Pryor and M. E. Flatté, Phys. Rev. Lett. **96**, 026804 (2006).
- ⁶ J. A. Brum and P. Hawrylak, Superlattices and Microstructures **22**, 431 (1997).
- ⁷ R. de Sousa and S. Das Sarma, Phys. Rev. B **68**, 155330 (2003).
- ⁸ H.-A. Engel, L. P.Kouwenhoven, D. Loss and C. M. Marcus, Quantum Information Processing **3**, 115 (2004).
- ⁹ L. S. Levitov and E. I. Rashba, Phys. Rev. B **67**, 115324 (2003).
- ¹⁰ J. Wang, H. Mao, J. Yu, Q. Zhao, H. Zhang, P. Yang, Z. Zhu and J. Chu, Appl. Phys. Lett. **96**, 062108 (2010).
- ¹¹ K. Chang, J. B. Xia, and F. M. Peeters, Appl. Phys. Lett. **82**, 2661 (2003).
- ¹² R. Rahman, S. H. Park, T. B. Boykin, G. Klimeck, S. Rogge L. C. L. Hollenberg Phys. Rev. B **80**, 155301 (2009).
- ¹³ A. De, C. E. Pryor and M. E. Flatté, Phys. Rev. Lett. **102**, 017603 (2009).
- ¹⁴ K. C. Nowack, F. H. L. Koppens, Y. V. Nazarov and L. M. K. Vandersypen, Science **318**, 1430 (2007).
- ¹⁵ T. Nakaoka, and S. Tarucha, and Y. Arakawa, Phys. Rev. B **76** 041301 (2007).
- ¹⁶ E. I. Rashba and A. L. Efros, Phys. Rev. Lett. **91**, 126405 (2003).
- ¹⁷ D. Loss, and D. P. DiVincenzo, Phys. Rev. A **57**, 120 (1998).
- ¹⁸ E. I. Rashba, Journal of Superconductivity **18**, 137 (2005).
- ¹⁹ I. Žutić, J. Fabian and S. Das Sarma Rev. Mod. Phys. **76**, 323 (2004).
- ²⁰ Y.-P. Shim, and P. Hawrylak, Phys. Rev. B **78**, 165317 (2008).
- ²¹ Y. A. Bychkov, and E. I. Rashba J. Phys. C: Solid State Phys. **17**, 6039 (1984).
- ²² G. Dresselhaus, Phys. Rev., **100**, 580 (1955).
- ²³ S. Takahashi, R. S. Deacon, K. Yoshida, A. Oiwa, K. Shibata, K. Hirakawa, Y. Tokura, and S. Tarucha, Phys. Rev. Lett. **104**, 246801 (2010).
- ²⁴ J. Pingenot, C. E. Pryor and M. E. Flatté Appl. Phys. Lett. **92**, 222502 (2008).
- ²⁵ C. F. Destefani and S. E. Ulloa, Phys. Rev. B **71**, 161303 (2005).
- ²⁶ O. Olendski, and T. V. Shahbazyan, Phys. Rev. B **75**, 041306 (2007).
- ²⁷ A. V. Khaetskii, and Y. V. Nazarov, Phys. Rev. B **61**, 12639 (2000).
- ²⁸ B. Schuh, J. Phys. A: Math. Gen. **18**, 803 (1985).
- ²⁹ V. Fock, Physik **47**, 446 (1928).
- ³⁰ C. G. Darwin, Proc. Cambridge Philos. Soc. **27**, 86 (1930).
- ³¹ Comsol Multiphysics version 3.5a (www.comsol.com).
- ³² A. J. Williamson, L. W. Wang, and A. Zunger, Phys. Rev. B **62** 12963 (2000).